ELSEVIER

Journal of Non-Crystalline Solids 221 (1997) 187–198

JOURNAL OF NON-CRYSTALLINE SOLIDS

Silver clustering in sodium silicate glasses: a molecular dynamics study

Dirk Timpel [a], Kurt Scheerschmidt [a,*], Stephen H. Garofalini [b]

[a] *Max Planck Institute of Microstructure Physics, Weinberg 2, D 06120 Halle, Germany*
[b] *Department of Ceramics, Rutgers University, Piscataway, NJ 08855-09009, USA*

Received 3 October 1996; revised 7 July 1997

Abstract

Molecular dynamics (MD) computer simulations with empirical potentials are applied to model the structure of sodium silicate glasses and the mobility of metallic particles enclosed. The particles are assumed to be generated by the Na–Ag ion-exchange, reducing the Ag ions and subsequent annealing. The theoretical investigations consider the modification of the glass structure owing to the ion exchange as well as the migration and clustering of the silver particles. Moreover, from the study of the migration processes we refine the empirical potentials applied to MD simulations and subsequent high resolution electron microscope (HREM) image calculations. © 1997 Elsevier Science B.V.

PACS: 61.16; 61.43; 61.46

1. Introduction

The physical properties of glasses are affected by the formation of metallic inclusions. Nanometer-sized crystalline Ag particles in alkali silicate glasses cause coloration, change the polarization and affect the mechanical properties of the glass depending, for example, on size and shape, distributions of the particles and their distribution in a glass. The particles can be generated by a sodium-silver ion exchange, thermally activated migration and subsequent annealing. The experiments are based on commercial glass consisting of 72% SiO_2, 13.8% Na_2O, 6.5% CaO, 6.0% MgO, and some other constituents, for example, 0.13% Fe_2O_3, which is important for the reduction of the Ag ions. Such glasses are ion exchanged in a $NaNO_3/AgNO_3$ liquid at 400°C. Subsequent annealing at temperatures between 460 and 600°C creates Ag particles $\leq$ 120 nm in size [1].

X-ray and neutron diffraction as well as EXAFS has been used to investigate the average structure of an ion-exchanged glass, i.e. the pair distribution (PDF) and the coordination numbers [2,3]. In addition, high resolution electron microscope investigations (HREM) provide local structural information at the atomic level, which indicate that the local glass structure alters the particle properties. In particular, HREM experiments show that, with decreasing particle diameter, the lattice parameters of the particles

* Corresponding author. Tel.: +49-345 558 2910; fax: +49-345 551 1223; e-mail: schee@mpi-halle.mpg.de.

PII S0022-3093(97)00333-5

decrease more strongly than expected for free particles [4].

This effect was recently proved by generating structural models of sodium silicate glasses and embedded silver particles applying molecular dynamics (MD) and molecular statics calculations [5,6]. Furthermore, a possibility was discussed of using HREM to visualize the structural modifications produced by relaxations on the basis of simulated HREM micrographs [7].

The described process of particle generation starting with an ion exchange in glass is complex and time-consuming so that MD simulations of the entire process seem to be inappropriate. Thus, the process is divided into subprocesses with a short time scale which then can be modelled by MD, i.e. first, the diffusion and the starting agglomeration of Ag within an ion-exchanged silicate glass, second, the growth and affects of extended Ag clusters on the glass. The complexity of the system, that means the large number of components, implies a problem somewhat more difficult. Therefore in a first step the problem is reduced to a sodium–silver ion exchange within a simple sodium di- or trisilicate glass. However, for this system problems arise in describing the particle interactions. For silicate, sodium silicate glasses as well as metallic structures there exist well-proven empirical and semi-empirical potentials [8–17]. The embedding of Ag within glass, however, has not yet been presented by MD, to our knowledge.

Because of the large number of degrees of freedom which arise from the empirical description of an interaction, in this paper the potentials and the parameters for the silver/glass interactions are varied to enable one to modify the glass structure as well as the Ag clustering process. The data determined from these variational procedures, which seem to fit known experimental measurements, are expected to describe the interaction appropriately. The aim of this paper and of a forthcoming one, which will describe the diffusion process in more detail, is to find the quantified potential most suitable for these interactions. At this stage, it is still not known whether the sodium/silver ion exchange, the diffusion of ions and atoms and the process of forming the agglomeration of the silver modify the glass matrix. The mobility of silver as well as the formation of silver clusters should also be included in the modeling.

2. Computational procedure

2.1. Molecular dynamics simulations

For a study of multi-component structures and their long-time dynamical behaviour the classical MD with empirical and semiempirical potentials is employed. The MD simulation starts with an energetically favourable structural model, for instance: with crystalline structures (e.g. α-$Na_2Si_2O_5$) for disilicates and with suitable stoichiometric modifications for trisilicates [8] and a Boltzmann distribution of particle velocities at an initial temperature. The numerical integration of the equations of motion determines the dynamics of the system.

The MD calculations were carried out with constant particle numbers, N, and a constant volume under periodic boundary conditions in all directions. The classical $3N$ Newtonian equations of motion were integrated with an integration step of 1 fs using the Nordsieck–Gear algorithm [18]. To control the system temperature the particle velocities were rescaled after 100 to 500 time steps. The MD simulations were made on extended structures using about 12 000 atoms, regularly updating neighbour lists and using a linked cell algorithm [19]. In addition, the program code was vectorized, which, however, only slightly increased the speed of the calculation.

The description of all system properties would require the application of first principle quantum mechanics, which, however, is time consuming and limited to about 100 atoms. Approximations derived from quantum mechanics, as, for example, tight binding or, at least, order-N methods imply fewer computational efforts than the direct first principle methods, but, at present they are applicable solely to two or three componential covalent structures. The empirical potentials applied here and enhanced by additional fit to diffusion properties will later on be refined by tight-binding approximations.

For describing a silicate glass structure or a pure metal, well established and proved interaction potentials are available [9–16]. However, for the silver glass interaction there are no reliable potentials and potential parameters so that several respective empirical potentials were tested with their parameters fitted to describe structural modifications of the ion-exchanged glass and the mobility of the enclosed silver particles.

The study is based on a well-known empirical SiO_2 potential which combines the modified Born–Mayer–Huggins (BMH) potential for ionic interactions with a weak three-body interaction term [14]. The two-body BMH interaction given by

$$U_{ij} = A_{ij} e^{-r_{ij}/\rho_{ij}} + \frac{Z_i Z_j}{4\pi\varepsilon_0 r_{ij}} \operatorname{erfc}\left(\frac{r_{ij}}{\beta_{ij}}\right) \quad \text{(I)}$$

(r: separation between atoms i and j; Z: formal ionic charge; A, ρ and β: parameters of strength, asymptotics and screening, respectively, to fit energy and minimum distances) consists of a short-range repulsion and a screened Coulomb term. In recent simulations this method, described in Ref. [15], was successfully applied to (see, for example, Refs. [9,16,20]) vitreous silica, silica–alumina interfaces and sodium silicate glasses. The three-body term is similar to that initially developed by Stillinger and Weber for silicon [14].

The Ag–Ag interaction is represented by a suitably fitted Lennard-Jones (LJ) potential (similar to Ref. [21]) or an embedded atomic method (EAM, [13]) potential, which, unlike LJ, allows a description of the surface and bulk properties of a metal. The silver was included in the silicate glass structure by applying either the 12-6-Lennard-Jones (LJ) potential to the Ag–O, Ag–Si and Ag–Na interactions, or applying a modified Born–Mayer–Huggins (BMH) potential. The pure two-body LJ-potential is given by

$$U_{ij} = 4\varepsilon_{ij}\left[\left(\frac{\sigma_{ij}}{r_{ij}}\right)^{12} - \left(\frac{\sigma_{ij}}{r_{ij}}\right)^{6}\right], \quad \text{(II)}$$

where ε_{ij} is the bonding strength between atoms i and j, σ_{ij} is the atomic interaction radius and r_{ij} is the separation between particles i and j. For the parameters see Table 1.

2.2. Calculations

The systems were simulated for 100 ps, applying a temperature regime as following (cf. Fig. 4, upper part). Starting at a constant temperature of 300 K, the temperature was increased in 4 ps to the annealing temperature at which it was kept constant over 22 ps. Afterwards, in 17 ps the system was cooled to the starting temperature before the annealing cycle was repeated.

The pair distribution function (PDF) was calculated at constant temperatures. The calculations, mostly based on a sodium trisilicate glass of 1536 atoms, were carried out for either a small (1.69 g/cm^3) or a large glass density (2.41 g/cm^3) according to a high and a low temperature limit, respectively, or for a density varying with temperature (quadratic fit [22]). The sodium/silver ion exchange in the relaxed model was performed at 0 K by randomly replacing 30% (in some cases 40 to 60%) of the sodium atoms by silver. This model approximately represents the experimental situation after the ion exchange and a diffusion of the Ag^+ ions which yields an approximately uniform distribution of Ag^+ within the glass matrix. Unlike experiments where, depending on the number of reducing agents available, part of Ag^+ is reduced to Ag, in the MD simulations it is assumed that all the Ag^+ will be reduced. Hence, the simulations start with Ag atoms in glass, the tendency of which to form clusters should be investigated here. The various Ag–glass/Ag–Ag interactions were used to investigate the effects of the silver atoms on the glass structure as well as clustering of the silver atoms. A selection of MD annealing simulations is given in Table 2. The MD simulations without additional comments are carried out using the standard parameter set, i.e. a small glass density and a maximum annealing temperature of T_{max} = 2500 K. The standard assumptions are given in Table 1.

Table 1
Standard parameter sets of potentials used: Lennard–Jones (LJ), Born–Mayer Huggins (BMH) and embedded atomic modification (EAM)

		Ag–Ag	Ag–O	Ag–Si	Ag–Na
LJ	ε (eV)	0.3446	0.1723	0.1498	0.03745
	σ (nm)	0.254	0.188	0.1917	0.218
BMH	A (eV)	–	1128.7	1560.0	3530.0
	β (nm)	–	0.234	0.230	0.230
	ρ (nm)	–	0.029	0.029	0.029
EAM		Ref. [12]	–	–	–

3. Results

3.1. Structure: pair distributions

To investigate the structure of the glass model, different PDFs are calculated by evaluating the trajectories at 100 K. This procedure enables us to compare the sodium silicate glass to the ion-ex-

changed one, thereby revealing the next neighbour distances as well as the coordination numbers. For comparison with experiments [2,3], the total PDF of the ion-exchanged sodium trisilicate glass structure of simulation 044 (see Table 2) is presented in Fig. 1. The peaks of the total PDF can be analyzed directly using the more detailed structural information gained from the partial pair distribution functions: Fig. 2 reveals the basic glass structure and Fig. 3, the silver environment.

With Figs. 1–3 the results of PDF analyses of all MD simulations can be summarized as follows.

(1) The silicate glass is dominated by the first Si–O peak at 0.161 nm, the O–O one at 0.261 nm and the Si–Si one at 0.317 nm.

(2) Si has a fourfold oxygen coordination (3.33 bridging and 0.67 non-bridging oxygen). Every SiO_4 tetrahedron is surrounded by ~ 3.5 other tetrahedra. The network modifying Na is coordinated by 3 to 5 oxygens (Na–O peak at 0.24–0.25 nm) and 2 to 4 Na (Na–Na peak at ~ 0.35 nm). The structure of the enclosed Ag is clearly indicated by the Ag–Ag and the Ag–O coordinations. Besides the formation of Ag clusters, it is generally assumed that Ag and O form Ag_2O-like structures. Some potential and parameter configurations can be interpreted to show this in the calculation. However, the simulations have shown that the silver environment depends on the silver interaction potentials chosen (cf. details of corresponding coordination numbers in Tables 3 and 4), which does not apply to Na.

(3) Besides a first peak there are also a second and partly a third one in all partial PDF, indicating higher coordination spheres.

(4) The structure of the silicate glass is only slightly affected by the Na–Ag ion-exchange and the Ag interaction potentials chosen. Table 3 demonstrates the sodium environment of the different MD simulated glass structures. The comparison of PDFs shows that the sodium environment is affected by the

Table 2
Outline of MD simulations (selected examples)

Na–Ag ion-exchange rate (%)	Ag–Ag	Ag–O	Ag–Si	Ag–Na	MD simulation
0	–	–	–	–	001 (ρ_{low}), 026 (ρ_{high})
30	EAM	LJ	LJ	LJ	011
30	EAM	LJh	LJh	LJh	013
30	EAM	LJd	LJd	LJd	012
30	EAM	LJ	BMH	LJ	010
30	EAM	LJh	BMH	LJh	010
30	EAM	Ljd	BMH	LJd	002 (T_{max} = 1500 K), 005 (T_{max} = 2000 K), 006 (T_{max} = 1000 K), 007 (T_{max} = 2500 K), 008 (T_{max} = 3000 K), 027 (ρ_{high})
30	EAM	BMH	BMH	LJd	034 (ρ_{var})
30	EAM	BMH	BMH	BMH	035 (ρ_{low}), 044 (ρ_{var})
30	EAM	BMH	BMH	BMH	044
30	LJ	LJ	LJ	LJ	014, 018 (r_c = 1 nm), 038 (T_{max} = 1500 K), 039 (T_{max} = 2000 K), 040 (T_{max} = 3000 K)
30	LJh	LJ	LJ	LJ	015
30	LJd	LJ	LJ	LJ	016, 041 (T_{max} = 1500 K), 042 (T_{max} = 2000 K), 043(T_{max} = 3000 K)
30	LJ	LJh	LJh	LJh	036
30	LJ	LJd	LJd	LJd	037
30	LJ	LJ	BMH	LJ	017
40	EAM	LJd	BMH	LJd	028
40	EAM	BMH	BMH	BMH	045
50	EAM	LJd	BMH	LJd	029
50	EAM	BMH	BMH	BMH	046

EAM: embedded atomic potential; BMH: modified Born–Mayer–Huggins potential; LJ: Lennard-Jones-potential with standard parameters; LJh: Lennard-Jones-potential with $\varepsilon/2$ bonding strength; Ljd: Lennard-Jones-potential with 2ε bonding strength; T_{max}: maximum annealing temperature; r_c: cut-off radius for LJ potential.

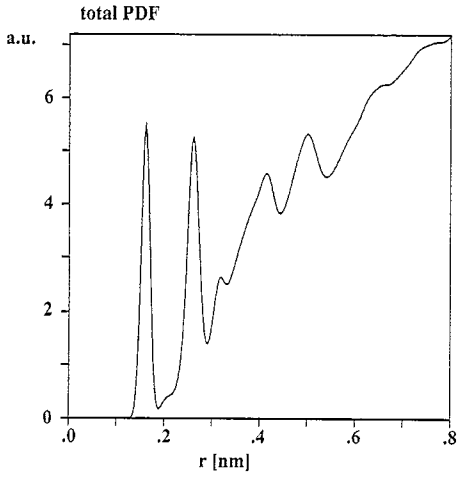

Fig. 1. Total pair distribution function of 30% Na–Ag ion-exchanged sodium trisilicate glass after 100 ps MD annealing (example 044 in Table 2).

variation of the glass density rather than by the ion-exchange. For all that, the inclusion of silver seems to result in a decrease of the first Na–Na coordination number whereas the sodium oxygen coordination solely reveals negligible changes.

(5) In Table 4 the results of the most important simulations are summarized to describe the Ag environment. The standard LJ parameters are fitted to

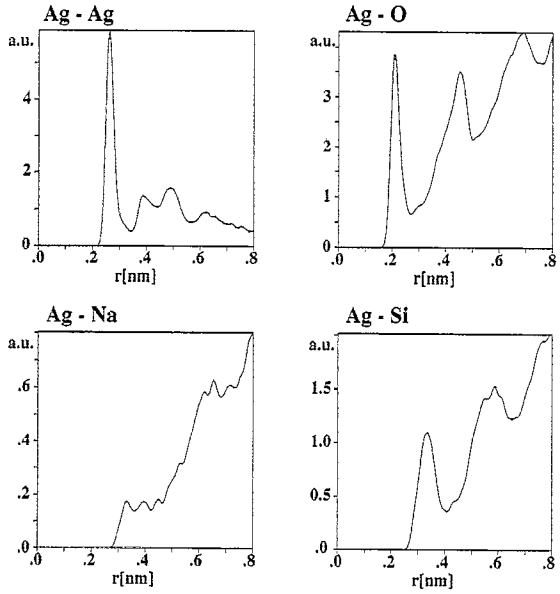

Fig. 3. Partial pair distribution function of the silver environment of 30% Na–Ag ion-exchanged sodium trisilicate glass after 100 ps MD annealing (example 044 in Table 2).

represent the equilibrium Ag–Ag and Ag–glass distances. A modification of the bonding strength, ε, causes changes of the next neighbour distances, but may result in a rearrangement of silver coordinations. A reduction ($\varepsilon/2$) of the Ag–Ag bonding

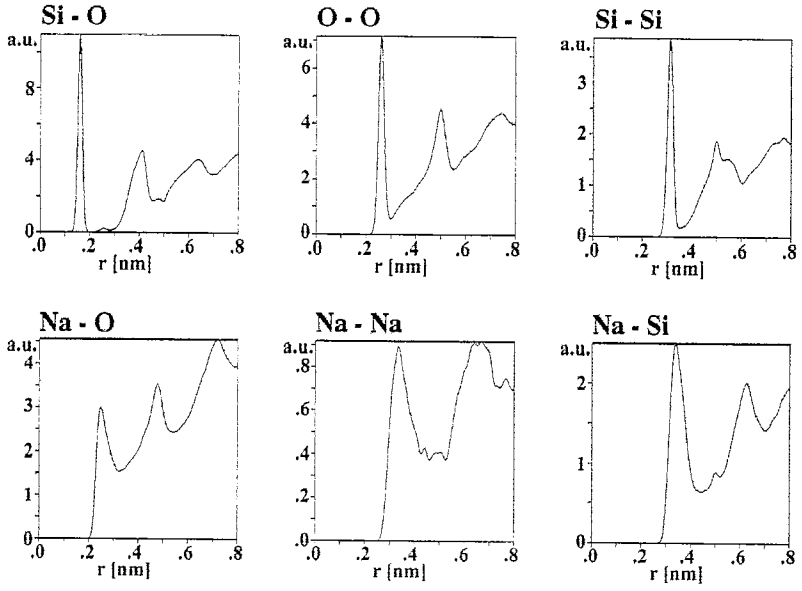

Fig. 2. Partial pair distribution function of the basic glass structure of 30% Na–Ag ion-exchanged sodium trisilicate glass after 100 ps MD annealing (example 044 in Table 2).

Table 3
Sodium environment, comparison of next-neighbour distances d (nm) and coordination numbers cn in sodium trisilicate glass, r_C: cut off radius of cn (selected examples, see text and cf. Table 2)

Potential: Ag–Ag/Ag–glass	d(Na–Na)	cn(Na–Na) (r_c = 0.41 nm)	d(Na–O)	cn(Na–O) (r_c = 0.32 nm)
-/-/(001)	0.360	2.6	0.240	3.6
-/-/(026)	0.343	3.7	0.250	5.6
LJ/LJ/(014)	0.360	1.8	0.239	3.5
LJh/LJ/(015)	0.360	1.8	0.238	3.5
LJd/LJ/(016)	0.344	2.1	0.241	3.4
LJ/LJh/(036)	0.357	1.8	0.239	3.6
LJ/LJd/(037)	0.338	1.9	0.239	3.6
EAM/LJ/(011)	0.350	1.7	0.238	3.6
EAM/BMH/(044)	0.330	1.8	0.240	3.5
Exp. in Refs. [2,3]			0.235	3.5
Exp. in Ref. [22]			0.232	4.3

strength (LJh_{Ag-Ag}) and an increase (2ε) of the Ag–glass bonding strengths ($LJd_{Ag-glass}$) have nearly the same effects on the structure: decreasing Ag–Ag coordination and increasing Ag–O. Doubling the Ag–Ag bonding strengths (LJd_{Ag-Ag}) and correspondingly reducing the Ag–glass bonding strength ($LJh_{Ag-glass}$) yield the opposite effect, viz. the enlargement of the Ag–Ag coordination and a decline of the Ag–O coordination. However, for LJd_{Ag-Ag} this behaviour is far more strongly revealed. The EAM simulated systems also show the formation of large Ag–Ag coordinations, however, connected with a slight shift of the first Ag–Ag peak of the partial PDF towards smaller distances. Associated with the BMH Ag–glass interaction, these systems also reveal an Ag–O coordination which corresponds quite well with experimental values [2,3].

3.2. Structure: Local glass topology

To investigate the influence of ion exchange on the silicate glass structure, silicon–oxygen arrangements have been studied in more detail, by counting the number of bridging oxygen atoms surrounding a silicon atom. The silicon atom of type Q_n is bonded to n bridging oxygen atoms.

Assuming, for comparison, a simple, but incorrect model (a gedanken experiment) of sodium uniformly distributed in a silicate network each sodium atom added produces a non-bridging oxygen, i.e. one Q_3.

Table 4
Silver environment, comparison of next-neighbour distances d (nm) and coordination numbers cn in sodium trisilicate glass, r_C: cut off radius of cn (selected examples, see text and cf. Table 2)

Potential: Ag–Ag/Ag–glass	d(Ag–Ag)	cn(Ag–Ag) (r_c = 0.35 nm)	d(Ag–O)	cn(Ag–O) (r_c = 0.26 nm)
LJ/LJ/(014)	0.281	2.44	0.207	4.4
LJh/LJ/(015)	0.277	1.2	0.209	5.0
LJd/LJ/(016)	0.281	6.02	0.205	2.9
LJ/LJh/(036)	0.282	2.99	0.204	3.4
LJ/LJd/(037)	0.277	1.7	0.207	5.4
EAM/LJ/(011)	0.270	3.6	0.205	4.1
EAM/BMH/(044)	0.261	3.9	0.213	2.8
Exp. in Refs. [2,3]	0.264–0.270	–	0.208–0.223	2
Exp. in Ref. [22]			0.208	2.1

Each silicon atom has to be bonded to not more than one non-bridging oxygen until all Q_4 are converted to Q_3. Thus in such a model of sodium trisilicate glass there have to be 33% of Q_4 and 67% of Q_3, but no Q_2 or Q_1. A thermodynamic description of the Q_n distribution within an alkali silicate glass is given by Gurman [21]. Thermodynamically, for the reactions

$$2Q_n \Leftrightarrow Q_{n-1} + Q_{n+1} \quad \text{(III)}$$

the equilibrium is described by

$$\frac{n_4 n_2}{n_3^2} = \frac{n_3 n_1}{n_2^2} = \frac{n_2 n_0}{n_1^2} = e^{-2\Delta E/kT}. \quad \text{(IV)}$$

ΔE is a bond ordering energy and T denotes the glass transition temperature. For $\Delta E \ll kT$, a random distribution results, for $\Delta E \gg kT$, the resulting step model is equivalent to our gedanken experiment. Values of $\Delta E/kT$ for different alkali glasses are fitted to experimental data, depending on the type of the alkali metal and the glass transition temperature but not on the concentration of the metal. Particularly for sodium silicate glasses in Ref. [23] the value of $\Delta E/kT = 2.5 \pm 0.5$ is given.

Besides small deviations our simulations show a general agreement with NMR and XPS investigations [24–26] enabling one to determine the relative proportion of different types of silicon atoms. In all simulations, Q_4 is dominating. Table 5 shows the values of Q_n as functions of the simulation parameters. The bridging fractions, Q_4, are always larger, and Q_3 always smaller than for the ideal model, which is the reason why additional fractions Q_1, Q_2, and Q_5 occur. The fraction of Q_2 corresponds quite well with the experimental values. In contrast to the experiment, in our simulations the fraction of Q_3 is smaller than that of Q_4, which is due to a small fraction ($\sim 2\%$) of Q_1. The glass structure with the higher density (026) has a small fraction of Q_5,

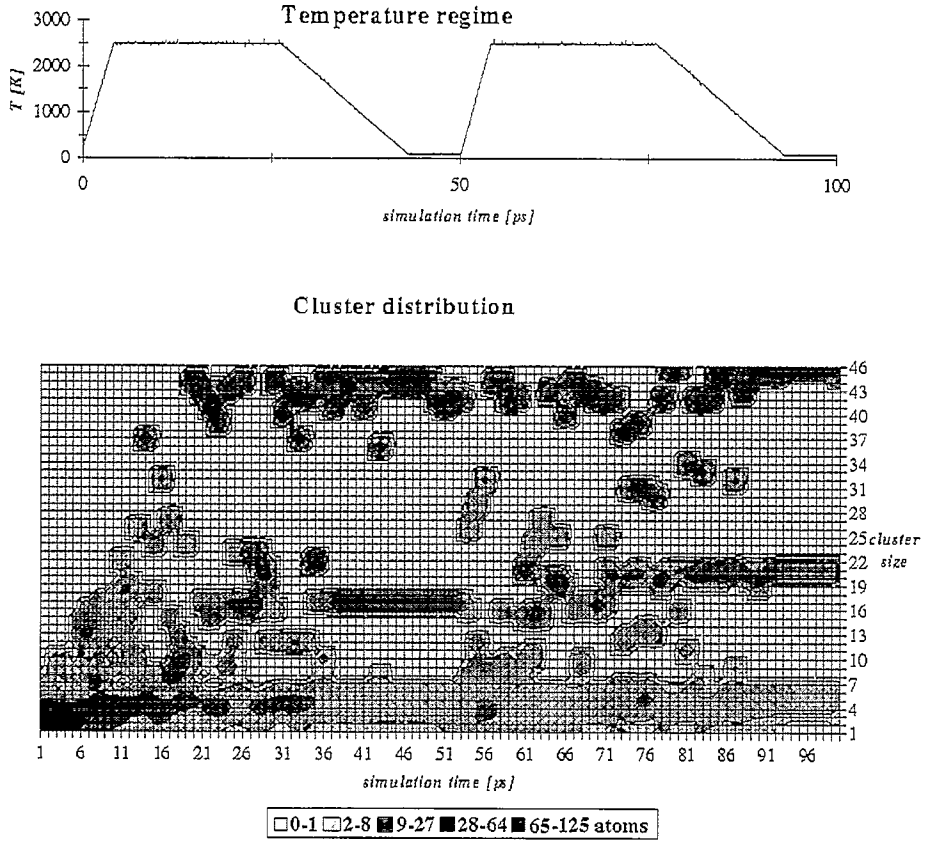

Fig. 4. Cluster distribution during 100 ps MD annealing for 30% Na–Ag ion-exchanged sodium trisilicate glass. The grey scale indicates the distribution of Ag atoms per cluster size.

Table 5
Distribution of the Q_n species (Si with n bridging oxygen) for different examples

Potential: Ag–Ag/Ag–glass	Q_1 (%)	Q_2 (%)	Q_3 (%)	Q_4 (%)	Q_5 (%)
-/-/(001)	1.1	10.9	41.9	46.1	0.0
-/-/(026)	0.3	10.2	40.4	45.6	3.6
LJ/LJ/(014)	1.8	12.2	36.7	49.2	0.0
LJh/LJ/(015)	1.3	10.9	40.9	46.9	0.0
LJd/LJ/(016)	1.3	11.2	39.8	47.1	0.5
LJ/LJh/(036)	1.0	12.8	38.0	48.2	0.0
LJ/LJd/(037)	2.3	9.1	41.4	47.1	0.0
EAM/LJ/(011)	1.3	9.6	43.2	45.6	0.3
EAM/BMH/(044)	1.3	12.0	38.5	48.2	0.0
LJ/LJ/(018)	0.3	6.3	30.7	43.5	18.5
Exp. in Ref. [20]	0.0	11.3	49.6	39.1	0.0

indicating that this system is not fully equilibrated. For longer simulations of about 500 ps this fraction vanishes. The sodium–silver ion exchange causes minor changes of the proportion of Q_n. The doubling of the LJ cut-off radius also tested, however, causes a large proportion of Q_5 indicating the destruction of the glass network.

According to Gurman's model [23] (Eq. (IV)) the equilibrium constants for our basic sodium di- and trisilicate glass models after 2 ns MD simulations are $\Delta E/kT \approx 0.7$ and 0.6, respectively. These results, however, are related to the theoretical glass transition temperature of approximately 3500 K as usually occurring in MD simulations, which is the most uncertain value of the calculations. Thus, the corrected values of $\Delta E/kT$ approximately correspond to 3.0 and 2.5, which both are slightly larger than the experimental values.

3.3. Clustering

The Ag–Na ion exchange without annealing results in isolated Ag atoms having coordination numbers less than those of the Na. For weak LJ Ag–Ag potentials compared to the standard parameters in Table 1, the annealing process only slightly affects this arrangement (e.g. 015 in Table 4). For a strong

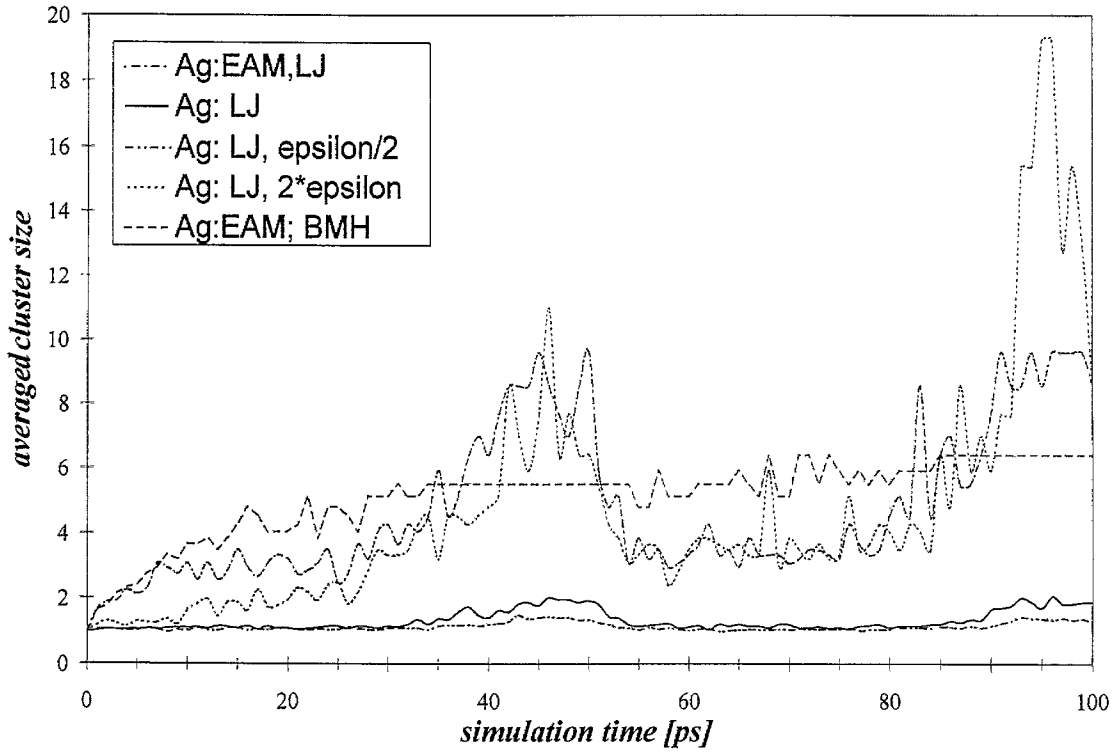

Fig. 5. Average cluster size versus simulation time for different Ag–Ag interactions for 30% Na–Ag ion exchanged sodium trisilicate glass.

LJ Ag–Ag interaction potential (LJd_{Ag-Ag}) or an EAM the Ag atoms tend to form clusters during annealing. Such a behaviour, experimentally observed for reduced Ag ions in glass, was investigated as a function of the interaction potentials as well as of the thermodynamic conditions. Fig. 4 reveals the cluster distribution during annealing for 100 ps. The cluster size is a function of the annealing time. The grey scale indicates how many Ag atoms altogether are included in the corresponding cluster size, i.e. the number of clusters in the respective class (e.g. if there are three clusters of always 16 atoms this results in the grey value of altogether 48 atoms). At the very beginning there are only isolated atoms or clusters of two atoms. Increasing the temperature causes the formation of clusters, with the size and number of the latter increasing until there is only a small number of non-clustered atoms. Cluster formation depends on the Ag potentials chosen. However, it is also affected by thermodynamic conditions such as maximum annealing temperature and glass density. To determine the dependencies, the averaged cluster size is introduced as a measure of cluster distribution. For identical ion-exchanged glass structures, annealing regime, and Ag-glass potentials but various Ag–Ag interactions, the clustering behaviour is shown in Fig. 5. With the LJ bonding strength as well as the cut-off radius being varied, EAM was additionally applied. Increasing the cut-off radius did not show any effect. Below a bonding strength of the standard LJ parameters (Table 1) solely a large number of very small clusters formed. Applying EAM and a strong LJ (2ε: LJd_{Ag-Ag}) caused the formation of larger clusters. Compared to LJ, EAM causes a faster formation of clusters starting already during heating. Besides, particles simulated with the LJ interaction are less stable and may decay owing to the heating process of the second annealing cycle. The Ag–glass interaction, too, affects the formation of Ag-clusters, but this effect is much smaller. Thus, the reduced bonding strength ($LJh_{Ag-glass}$) as well as the standard parameters of the Ag–O bonds, for instance, cause a stronger clustering (see examples 016 and 036 in Table 4).

In Fig. 6, again showing clustering versus simulation time, the maximum annealing temperature is varied, whereas the other system parameters are kept constant in all simulations. For an Ag–Ag interac-

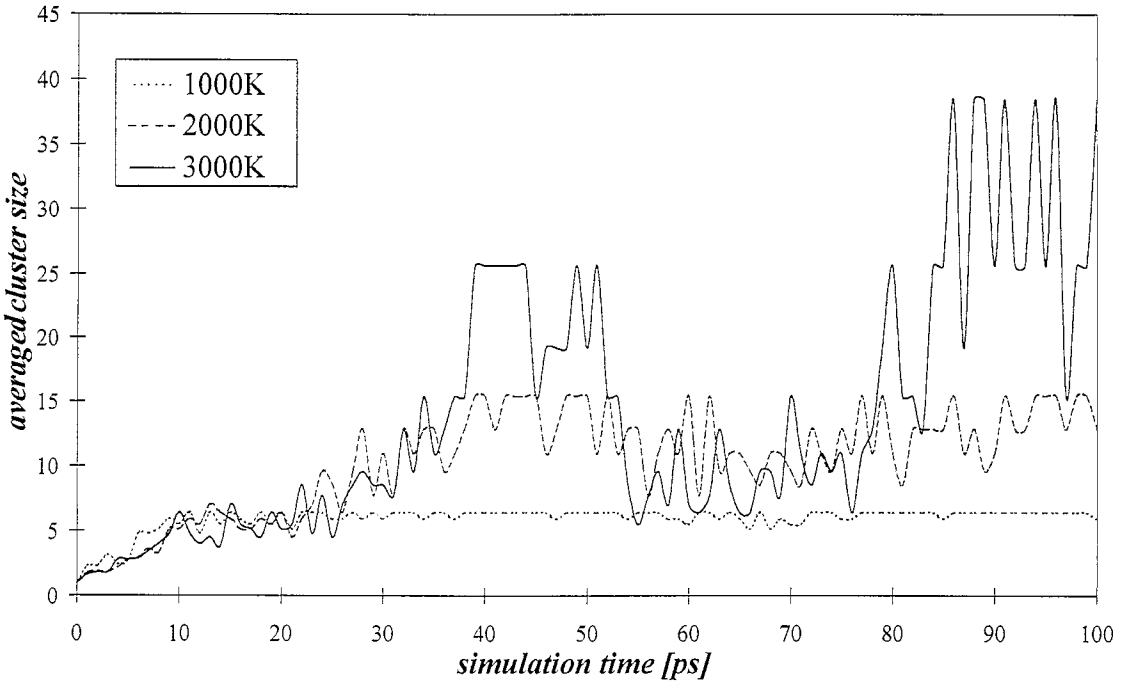

Fig. 6. Average cluster size versus simulation time for different maximum annealing temperatures for 30% Na–Ag ion exchanged sodium trisilicate glass.

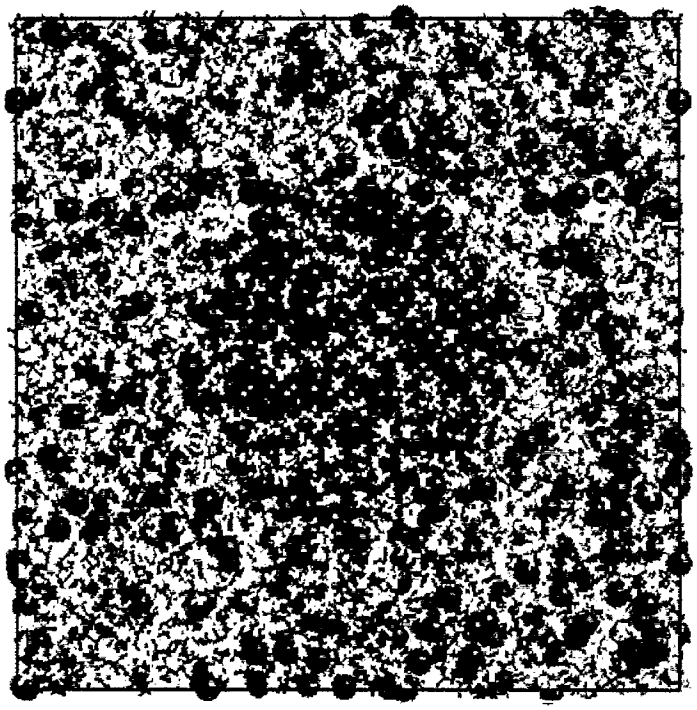

before

a)

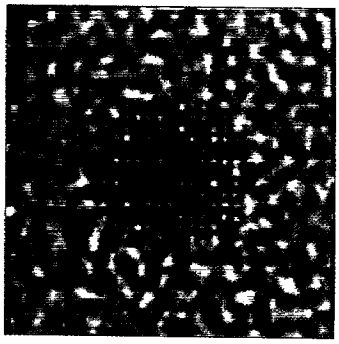

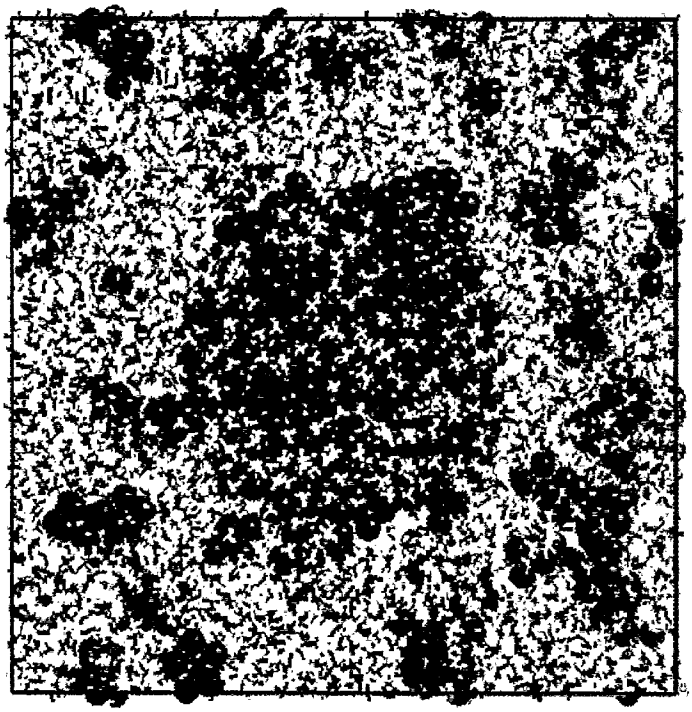

after

b)

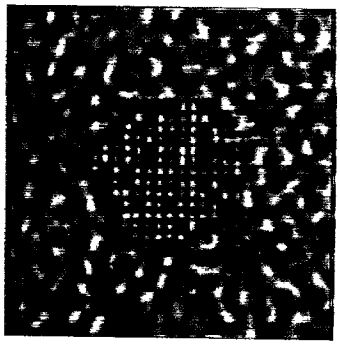

tion, simulated with EAM or with LJ with standard parameters or doubled bonding strength, higher annealing temperatures yield larger clusters.

In addition to the formation of small Ag clusters starting with a uniform distribution of the Ag atoms we have also treated larger crystalline Ag precipitates of about 2000 atoms in glass. Such particles are of special relevance because of their experimental accessibility as, for example, by means of HREM. Because of the limited calculation time (100 ps for systems of 10000 atoms) it seems impossible to generate such large particles directly as a result of MD simulations. Therefore the precipitates are artificially included in a relaxed glass structure. The procedure and the resulting structures are described in Ref. [7] and can be summarized as follows: A spherical hole is cut into a well relaxed glass matrix. Afterwards, a crystalline Ag particle, also spherical, of a diameter slightly smaller than the hole is included in the latter. Subsequently, the whole structure is MD simulated with the particle kept frozen for a couple of steps to reconstruct the particle–matrix interface.

Fig. 7 shows an example of MD simulations for a sodium trisilicate glass model of 12288 atoms (6.25 $\times$ 6.25 $\times$ 6.25 nm) together with calculated HREM images. Besides the 30% Na–Ag ion exchange, spherical crystalline Ag particles of 1048 atoms are included in the model. Thus, the growth of larger sessile particles due to the agglomeration of mobile smaller aggregates can be studied, which represents an advanced state of the whole physical clustering process. Such a mixed model is developed to analyze the imaging effects and to prove the visualization of clusters and of smaller and larger particles by simulating HREM micrographs. Fig. 7a shows the structural model before annealing and the corresponding simulated HREM micrograph. In the glass matrix the exchanged silver is almost randomly distributed. In the centre of the model the precipitate is situated. In the HREM image, the crystalline particle detectable by its lattice fringes clearly stands out against the speckled contrast of the amorphous matrix.

Annealing for 100 ps at a maximum temperature of 1000 K results in the formation of small particles of up to 50 atoms. Besides, the large crystalline precipitate is growing with its surface changing (Fig. 7b). The change in particle shape is indicated by the HREM contrast as discussed in Ref. [7]. Besides, there are contrast correlations caused by the small Ag clusters in the matrix. Most of the smaller clusters, however, cannot be resolved in the HREM images.

4. Discussion

Experimental and simulated HREM micrographs demonstrate the visibility of larger particles ($>$ 100 atoms) and their structural changes (shape modifications and relaxation). The quantitative analysis of the properties and the structural behaviour, studied by MD simulations, is affected by the glass structures as well as particle mobility and the interaction of both. The MD simulations of migration and clustering, however, depend on the interaction potentials chosen: The structure of the sodium trisilicate glass were found to be determined by the existence of pure SiO_2 regions and sodium channels through the glass (large proportions of Q_4 and Q_2 relative to our gedanken experiment as well as the sodium coordination). The silicate network structure was not affected by the Na–Ag ion-exchange (no significant changes of the Qn Distribution). The first Na–Na coordination number seems to reveal a minor decrease caused by the inclusion of silver. The silver species do not simply occupy the sodium sites but form another environment, which depends on the silver interaction potentials chosen. The EAM simulated systems show an Ag–Ag coordination which indicates the formation of compact clusters, additionally connected with a decrease of the Ag–Ag next neighbour distance. Associated with the BMH Ag–glass interaction, these systems also reveal an Ag–O coordination, which corresponds quite well with experimental values. Besides, applying EAM or a sufficiently strong LJ

Fig. 7. Spherical Ag-particle (1048 atoms) in 30% Na-Ag ion-exchanged sodium trisilicate glass (6.25 $\times$ 6.25 $\times$ 6.25 nm) before (a) and after (b) MD annealing with corresponding simulated HREM images (acceleration voltage $U = 400$ kV, spherical aberration $C_s = 1$ mm, defocus $\Delta = 70.0$ nm, defocus spread $\delta = 10$ nm, beam divergence $\alpha = 0.5$ mrad).

(2ε: LJd_{Ag-Ag}) causes the formation of larger clusters. Compared to LJ, EAM induces a faster formation of clusters starting during heating, resulting in more stable clusters, which do not decay during the second annealing cycle. Comparing the theoretical results with the experimental data from the literature thus yields:

(1) Glass structures comparable with experiments are described by simulation (044) and (014) (in Table 2).

(2) Simulation (044) and (016) (in Table 2) characterize the particle mobility and the formation of compact clusters.

(3) The most important features are the existence of channels in the network, and the silver clustering, which negligibly affects the silicate network.

5. Conclusions

Our MD generated model of an ion exchanged sodium trisilicate glass provides a MD description of structure and dynamics of silver in glass.

In the silicate network of sodium trisilicate glass the sodium species were found not to be uniformly distributed, indicating channel-like structures in the glass of increased sodium density. A comparison of the PDFs of the silver and sodium environments shows that silver forms a different environment not essentially changing the silicate network topology. Besides, silver has a strong tendency to form clusters, which mainly depends on the annealing regime and the Ag–Ag interaction potential. However, solely for the EAM simulated silver the Ag–Ag distances of the small clusters are reduced, which is predicted by HREM experiments. Based on experimental results for equilibrium distances, coordination numbers, bridging fractions and cluster extensions as functions of the potential structure and its free parameters a refinement of the empirical potentials applied to the MD simulations is made.

Acknowledgements

We are grateful to the Deutsche Forschungsgemeinschaft for financial support.

References

[1] K.-J. Berg, A. Berger, H. Hofmeister, Z. Phys. D 20 (1991) 313.
[2] M. Dubiel, G. Mosel, Jpn. J. Appl. Phys. 33 (1994) 5892.
[3] M. Dubiel, R. Schmitz, U. Kolb, D. Gutwerk, H. Bertagnolli, Phys. B 208&209 (1995) 349.
[4] H. Hofmeister, M. Dubiel, H. Goj, S. Thiel, J. Microsc. 177 (1995) 331.
[5] K. Scheerschmidt, D. Timpel, Optik 93 (Suppl. 5) (1993) 81.
[6] K. Scheerschmidt, D. Timpel, Electron Microscopy: Proc. 13, vol. 2A, ICEM Paris, 1994, p. 395.
[7] D. Timpel, K. Scheerschmidt, Phys. Status Solidi (a) 150 (1995) 51.
[8] S.H. Garofalini, S.M. Levine, J. Am. Ceram. Soc. 68 (1985) 376.
[9] H. Melman, S.H. Garofalini, J. Non-Cryst. Solids 134 (1991) 107.
[10] B. Vessal, A. Amini, D. Fincham, C.R.A. Catlow, Philos. Mag. B 60 (1989) 752.
[11] W. Smith, G.N. Greaves, J. Chem. Phys. 103 (8) (1995) 3091.
[12] S.M. Foiles, M.I. Baskes, M.S. Daw, Phys. Rev. B 33 (1986) 7983.
[13] G.J. Ackland, G. Tichy, V. Vitek, M.W. Finnis, Philos. Mag. A 56 (1987) 735.
[14] B.P. Feuston, S.H. Garofalini, J. Chem. Phys. 89 (1988) 5818.
[15] S.H. Garofalini, J. Non-Cryst. Solids 120 (1990) 1.
[16] R.G. Newell, B.P. Feuston, S.H. Garofalini, J. Mater. Res. 4 (1988) 434.
[17] A.R. Rosenthal, S.H. Garofalini, J. Am. Ceram. Soc. 70 (1987) 821.
[18] C.W. Gear, Numerical Initial Value Problems in Ordinary Differential Equations, Prentice Hall, New York, 1971.
[19] G.S. Grest, B. Dünweg, K. Kremer, Comp. Phys. Commun. 55 (1989) 269.
[20] S. Bionski, S.H. Garofalini, J. Phys. Chem. 100 (1996) 2201.
[21] S.M. Levine, S.H. Garofalini, J. Chem. Phys. 88 (1988) 1242.
[22] O.V. Mazurin, M.V. Streltsina, T.P. Shvaiko-Shvaikoskaya, Handbook of Glass Data, Physical Sciences Data, Elsevier, New York, 1983.
[23] S.J. Gurman, J. Non-Cryst. Solids 125 (1990) 151.
[24] H. Hater, W. Müller-Warmuth, M. Meier, G.-H. Frischat, J. Non-Cryst. Solids 113 (1989) 210.
[25] H. Maekawa, T. Maekawa, K. Kawamura, T. Yokakawa, J. Non-Cryst. Solids 127 (1991) 53.
[26] J.M. Inman, S.N. Houde-Walter, B.L. McIntyre, Z.M. Liao, R.S. Parker, V. Simmons, J. Non-Cryst. Solids 194 (1996) 85.